water

MDPI

Article

Monitoring Coastal Lagoon Water Quality through Remote Sensing: The Mar Menor as a Case Study

Manuel Erena [1,*], José A. Domínguez [2], Felipe Aguado-Giménez [3], Juan Soria [4] and Sandra García-Galiano [5]

1 IMIDA, GIS & Remote Sensing, 30150 Murcia, Spain
2 VURV, Crop Research Institute, 161 06 Prague, Czech Republic
3 IMIDA, Marine Aquaculture Station, 30740 San Pedro del Pinatar, Spain
4 Instituto Cavanilles de Biodiversidad y Biología Evolutiva, Universidad de Valencia, 46980 Paterna, Spain
5 Department of Mining and Civil Engineering, Universidad Politécnica de Cartagena, 30202 Cartagena, Spain
* Correspondence: manuel.erena@carm.es; Tel.: +34-968-366-751

Received: 4 April 2019; Accepted: 9 July 2019; Published: 15 July 2019

Abstract: The Mar Menor is a hypersaline coastal lagoon located in the southeast of Spain. This fragile ecosystem is suffering several human pressures, such as nutrient and sediment inputs from agriculture and other activities and decreases in salinity. Therefore, the development of an operational system to monitor its evolution is crucial to know the cause-effect relationships and preserve the natural system. The evolution and variability of the turbidity and chlorophyll-a levels in the Mar Menor water body were studied here through the joint use of remote sensing techniques and in situ data. The research was undertaken using Operational Land Imager (OLI) images on Landsat 8 and two SPOT images, because cloudy weather prevented the use of OLI images alone. This provided the information needed to perform a time series analysis of the lagoon. We also analyzed the processes that occur in the salt lagoon, characterizing the different spatio-temporal patterns of biophysical parameters. Special attention was given to the role of turbidity and chlorophyll-a levels in the Mar Menor ecosystem with regard to the programs of integral management of this natural space that receives maximum environmental protection. The objective of the work has been fulfilled by answering the questions of the managers: when did the water quality in the Mar Menor begin to change? What is happening in the lagoon? Is remote sensing useful for monitoring the water quality in the Mar Menor? The answers to these questions have allowed the generation of a methodology and monitoring system to track the water quality in the Mar Menor in real-time and space. The tracking system using satellite images is open to the incorporation of images provided by new multispectral sensors.

Keywords: Mar Menor; spatio-temporal variability; Landsat 8

1. Introduction

Since 1972, Landsat satellites have provided Earth Observation (EO) data to support assessments of natural and human-induced changes on the Earth, such as water science issues [1]. One of the aims of the use of Landsat images in water quality issues has been to obtain thematic mapper datasets [2]. The remote sensing advances of the last decade of the 20th Century and the first decade of the 21st Century facilitated the application of Landsat satellites images by water managers [3]. The future of remote sensing in water science is related to the observation, understanding, and prediction of the spatial and temporal distribution of water quantity and quality [4].

Water quantity monitoring has demanded the development of new sensors and platforms as well as new remote sensing methodologies [5], while water quality monitoring requires a good atmospheric

correction of the images of water bodies. This requirement has been achieved by several sensors, such as: Thematic Mapper (TM) images from Landsat 5 [6], Enhanced Thematic Mapper Plus (ETM^+) images from Landsat 7 [3], Operational Land Imager (OLI) from Landsat 8 [7], and MEdium Resolution Imaging Spectrometer (MERIS) images [8].

Remote sensing has been considered a good tool to improve water quality control, because information can be retrieved nearly every day in real-time by different sensors and platforms [9–11]. From the point of view of water pollution monitoring as well as management of inland and coastal waters, this ability is very valuable due to Water Framework Directive (WFD) requirements.

Due to the MERIS sensor switch-off, there was a gap in the images available for water quality monitoring. The Landsat 8 satellite was launched on 11 February 2013, then the use of the OLI and Thermal Infrared Sensor (TIRS) sensors installed aboard Landsat 8 began [12,13]. Simultaneously, the EU Copernicus program for EO and monitoring started to expand. Established in 2014, its Sentinel satellites bring continuity to the global monitoring for environment and security (GMES) program started in 2001 by the European Space Agency (ESA) [14,15].

The experience gained previously (until 2013) will allow researchers to know the steps to follow in this new stage (e.g., the corresponding atmospheric correction to be applied to each sensor; the correct selection of the sensor to be used). In the second step, new and improved algorithms could be developed in relation to the retrieval of water quality parameters (e.g., bands in the visible and near infrared region, as well as water absorption in the rest of the spectral ranges). Moreover, in the case of the chlorophyll-a algorithms, there is a need to consider separately the low and high concentrations, with their corresponding validations [8]. Once these methodologies have been consolidated, it will be possible to study time series and multi-scale data as well as specific events related to cyanobacteria in different water bodies [16].

Another possibility is to determine the types of inland and coastal waters in optical terms [17], in order to extract the spectral signatures defining the different ecological indicators such as bathymetry [10], macroalgae [18], and seagrass [16]. If the better spectral responses are known, our knowledge of water bodies' classification will be better [17,19].

Until the MERIS sensor switch-off, remote sensing techniques were widely applied. However, it is necessary to restore confidence in the new sensors, such as those of Landsat 8 [20], Sentinel-2 [21], and Sentinel-3 [22], and in the connectivity of the information from different sensors with field data and their information networks [23].

Several European countries use remote sensing techniques (e.g., Landsat images) to improve their management [8]. Spain began to use Landsat 5 images to assess issues in the Albufera Lagoon of Valencia [2]. One of the aims of the present work is to apply Landsat 8 images to assess several environmental issues of the Mar Menor Lagoon. This coastal lagoon is located in the Southeast of Spain and suffers several pressures, mainly produced by human activities. Therefore, the main aim of this work is to assess the use of remote sensing by developing a water operational monitoring system to study and understand what happens in the lagoon. This represents the first step in determining the cause-effect relationships, in order to satisfy the WFD requirements. The improvement in our understanding of the degradation processes occurring in the lagoon will be the basis on which to propose solutions to these problems in this fragile ecosystem, in near real-time and with the lowest possible cost. The decision-taking process undertaken by the water managers should be based on a robust knowledge of the processes that are occurring in the lagoon.

2. Study Area

The Mar Menor is a hypersaline coastal lagoon located in the semi-arid Murcia Region of southeast Spain (Figure 1). It occupies an area of approximately 135 km^2 and has a total volume of 6.53×10^8 m^3 at seawater level [24]. The depth in the lagoon reaches 7 m, with an average depth of 4 m. The Mar Menor constitutes a restricted littoral lagoon that is relatively isolated from the adjacent Mediterranean Sea, by a sandy bar (named La Manga) that is 20 km long, 100 to 900 m wide, and crossed by three

shallow channels (named Encañizadas del Ventorillo y La Torre, El Estacio, and Marchamalo). The lagoon is situated at the end of a watershed bordered by a group of mountain ranges that surround the Campo de Cartagena area, a wide agricultural plain of about 1440 km^2.

Figure 1. Location of the Mar Menor coastal lagoon, in the Murcia Region of the Iberian Peninsula, and ground-based data: red circles (weekly) and blue triangles (on 2 April 2017).

The main geomorphological elements that influence the lagoon dynamics are [24]: the sandy barrier; the inlets or 'golas'; the islands; the gullies (wadis); and the marginal lagoons. Freshwater inputs into the lagoon are restricted to six ephemeral watercourses called wadis (gullies or 'ramblas'). These are intermittent channels but are usually active during flood episodes, carrying flow and sediments. The Albujón wadi constitutes the largest watercourse and drains the adjacent agricultural area of Campo de Cartagena. It drains a surface area of 441 km^2, about one-third of the total area of Campo de Cartagena. The Los Alcázares wadi consists of a diffuse network of channels and it reaches the Mar Menor at the town of Los Alcázares [24]. The Miranda wadi consists of two main channels that converge diffusely in the El Carmoli salt marsh. The other three small wadis that reach the lagoon are the Beal, Ponce, and Carrasquilla wadis; occasionally, during storms, they carry metal wastes and mineral deposits from former mining areas located nearby.

The area has a semi-arid Mediterranean climate, characterized by warm and dry weather. The mean annual temperature ranges from 17 to 21 °C. Winters are mild, with minimum temperatures around 10–13 °C. Summer temperatures reach values above 25 °C. The annual precipitation is low (<300 mm yr^{-1}) and mainly occurs during storm events in fall and winter. There is almost no precipitation

during July and August, when the maximum evaporation rates are observed. The wind regimes in the area are dominated by the first and second quadrants, with a marked seasonal pattern: westerly winds dominate during autumn and winter, while winds from the northeast and southeast dominate during spring and summer [24].

The ecosystem of the Mar Menor has been transformed since the early 20th century [25], due to the setting-up of the Spanish Army base of seaplanes in 1915. Coexisting with this, fishing and traditional agriculture were the main economic activities of the area in the early 20th century. In the 1960s and 1970s, the area underwent a great transformation due to the development of tourism on the Spanish Mediterranean coast; La Manga, the area of land that separates the Mar Menor lagoon from the Mediterranean Sea, developed into one of the most attractive places for tourists, both in Spain and in the rest of Europe [26,27]. To all of this, one must add the industrial development and the mining activity that began in the time of the Romans to the south of the lagoon, in the Campo de Cartagena area. A new change took place in the last two decades of the 20th century, when the expansion of tourism was limited by that of the agricultural area, which has become one of the main areas of horticultural production in Europe [28], with several crops of vegetables and fruit each year regardless of the absence of water caused by the periods of drought that this part of Spain usually suffers from. All these pressures have caused a decrease in the natural spaces and a demand for the conservation of the environment from the public and environmental groups that wish to achieve a sustainable economy [29].

During the summer of 2015, there was a change in the apparent color of the water of the lagoon from blue to greenish; this became even more evident in early 2016. This provoked a protest from the tourism sector that extended to the whole population, worried by the bad state of the lagoon and its poor environmental management, which were obvious because of the degradation of the water quality—as manifested most clearly by a drastic change in transparency. In fact, it is not possible to see the beds of Neptune grass (*Posidonia* plants) from a boat [30] and the color of the water is now emphatically green [31].

The social pressure was such that the government of the Region of Murcia had to take action to calm the protests and demonstrations down and to study and monitor the water quality of the Mar Menor lagoon, to determine the causes-effects relationships that had led to that situation and thus to be able to undertake the appropriate actions to restore the ecosystem.

The managers of the Mar Menor considered two questions: when and why had this transformation taken place? The answers were not easy to find, because they required data from the past, which were not available to the managers of the Mar Menor at that moment. The use of satellite images arose in response to the need to conduct the research that the water managers needed in the shortest possible time, to address the absence of this information.

3. Materials and Methods

This section is divided into dataset collection (extra radiometric and water quality field data campaigns, besides several phytoplankton field data campaigns) and applied methodology, in order to improve our knowledge of the lagoon's processes.

3.1. Materials

(a) Ground-Based Data

On a weekly basis, and at 12 different points (Figure 1) covering all areas of the Mar Menor, the IMIDA (Murcian Institute of Agricultural Research & Development) field team obtained the profiles of the SBE 19plus CTD (Sea-Bird Electronics, WA, USA) parameter, turbidity, and chlorophyll-a concentration from May 2015 to October 2017.

An extra field data campaign was carried out on 2 April 2017. Five locations were selected for the collection of measurements, based on the preliminary results of the images analysis:

- Radiometric measurements were acquired using a Hobi Labs HidroRad-1 radiometer: $L_{wu}(0^+,\theta,\phi,\lambda)$ is the water-leaving radiance uncorrected for reflectance of downwelling light at the water surface. Sky radiance is denoted $L_{sky}(0^+,\theta,\phi,\lambda)$ and is measured at an angle θ away from the zenith axis. For a small acceptance angle, there is negligible dependence of *Lwu* on viewing angle θ (the same angle away from the zenith as for L_{sky}, but mirrored on the horizontal plane) and azimuth angle ϕ (away from the sun's azimuth), as long as $\theta < 42°$, for ϕ ranging from 90° to 135° [32,33]. The measurement geometry was kept within these limits and 30° < sun zenith angles < 60° were avoided in all cases. The skylight correction factor $r(\theta)$ can be approximated by a constant value for calm water surfaces or obtained as a function of wind speed and cloud cover [34]. The solar downward irradiance $Ed(0^-,\lambda)$ was measured just below the water surface, and the spectral solar downward irradiance $Ed(z,\lambda)$ was measured at depth z [35]
- Water quality measurements in vertical profiles were performed with a Turner C-3 profiler, on which were mounted three fluorometers to measure the chlorophyll-a concentration, phycocyanin, and turbidity.

Moreover, several phytoplankton field data campaigns were carried out from May to December 2017. The algal group composition of the phytoplankton was obtained from a sample fixed in Lugol's solution, for taxonomic identification and quantification. Cell counting and biovolume calculations were carried out using a Nikon inverted microscope, after sedimentation with Utermöhl's method After glass fiber GF/F (Whatman, GE Life Sciences, UK) filtration of each water sample, chlorophyll-a was extracted into acetone (90%) + Dimethyl sulfoxide (1:1); the extracts were clarified by centrifugation and measured by spectrophotometry [36].

(b) Satellite Data

Remote satellite images from two sensors and platforms were used to get high temporal resolution. From June 2015 to October 2017, 51 images from the Landsat-8 satellite and two from the SPOT-7 satellite were used. In the Supplementary Materials Figures S1–S3 show the dates of the selected images. Landsat-8 OLI images are available online at the United States Geological Survey (USGS) web page (https://earthexplorer.usgs.gov/), while SPOT-7 images were provided georeferenced and atmospherically corrected by Airbus.

3.2. Methodology

(a) Image processing

The atmospheric correction of OLI images was performed based on the Gilabert algorithm [6], which is appropriate for dark areas such as water bodies, shadows, and high-humidity areas. This atmospheric correction has been adapted for OLI images [7]. Its good performance, relative to other atmospheric corrections used for monitoring of the water quality of lakes and reservoirs, was shown when such data were compared with in situ radiometric data obtained using an ASD-FR spectroradiometer [37,38].

In order to focus the image processing on the Mar Menor water layer, a water/land pixel classification was performed using a simple threshold applied in the near infrared band [3].

The water quality parameters selected as eutrophic and pollution indices were the chlorophyll-a concentration ([Cla]) and water turbidity. Regression analyses were performed using atmospherically corrected true reflectance values of OLI bands downloaded from the USGS web page [12,39,40], and the time series of images were processed and analyzed to obtain the time series of each parameter. The images were processed with ENVI 4.8 remote sensing software (Harris Corporation. FL 32919, USA) [41].

Once the method had been fine-tuned, the processing was implemented as an ArcGIS script (ESRI, Redlands, CA, USA) installed in the IMIDA computer. The entire time was accounted for since the image is acquired by the sensor until the thematic map is delivered to the manager's server, in order to analyze the feasibility of a near real-time qualitative monitoring system [42].

(b) Likewise, the field data are divided into two topics:

a. Bio-physical water parameters.

The values of the turbidity and [Cla] at each point were calculated as the averages of the profile values in the first meter. These were used jointly with values from the OLI sensor to obtain the algorithms required to generate the thematic mapper.

b. Spectral data.

The water apparent optical properties—the water-leaving reflectance (R_w) and diffuse attenuation coefficient (K_d)—were calculated from on-site spectral measurements. The spectral measurements of $L_w(0^+,\theta,\phi,\lambda)$, $L_{sun}(0^+,\theta,\phi,\lambda)$, and $Ls_{ky}(0^+,\theta,\phi,\lambda)$ were carried out by adapting National Aeronautics and Space Administration (NASA) protocols [37]. The downward irradiance $Ed(0^+,\lambda)$ was calculated from $L_{sun}(0^+,\theta,\phi,\lambda)$.

$$L_w\,(0^+,\theta,\phi,\lambda) = L_{wu}(0^+,\theta,\phi,\lambda) - r(\theta)\cdot L_{sky}(0^+,\theta,\phi,\lambda) \quad (1)$$

$$R_w = \pi L_w(0^+,\lambda)/E_d(0^+,\lambda) \quad (2)$$

This methodology has been applied in several research projects involving the measurement of optical properties in the field [3,10,43–46]. The ratio between the water-leaving reflectance just above the surface, $R(0^+)$, and the water-leaving reflectance just below the surface, $R(0^-)$, corresponds to 0.544 [3,45,46].

The diffuse attenuation coefficient, $K_d(\lambda)$, of the spectral solar downward irradiance, $E_d(\lambda)$ [3,46], is defined by:

$$K_d(\lambda) = \ln\,[E_d(0^-,\lambda)/E_d(Z,\lambda)]/Z \quad (3)$$

The relationships between the apparent and inherent water properties are determined by:

$$R(0^-) = C(b_b/(b_b + a))\ 0.32 < C < 0.37;\ C = 0.32 \quad (4)$$

when the sun is at its zenith; and:

$$(K_d) = [a^2 + (0.47(\mu_0 - 0.218)ab]1/2/\mu_0 \quad (5)$$

$$b_b = 0.02b \quad (6)$$

where a is the absorption coefficient, b the scattering coefficient, b_b the backscattering coefficient, and μ_0 the cosine of the angle of incidence [47].

The total absorption coefficient is partitioned as follows:

$$a(\lambda) = a_{sw}(\lambda) + a_{ph}\,(\lambda) + a_{CDOM}\,(\lambda) + a_{NAP}(\lambda) \quad (7)$$

where the subscripts *sw*, *ph*, CDOM, and NAP designate, respectively, seawater (*sw*), phytoplankton (*ph*), the combined contribution of colored dissolved organic matter (CDOM), and non-algal particulate (also detrital) matter (NAP); the absorption is not separated owing to the similarities in the spectral shapes of the components [48–51].

The CDOM absorption decreases exponentially according to the following equation:

$$a_{CDOM}(\lambda) = a_{CDOM}(\lambda_o)\cdot\exp[-S_{CDOM}(\lambda - \lambda_o)] \quad (8)$$

where S_{CDOM} is the slope factor and λ_o is the reference wavelength, nominally 440 nm. The slope factor of a_{CDOM} was derived through nonlinear curve fitting between 412 nm and 510 nm (including the reference data set, see below). As such, the slope values presented here are used as a metric to compare the CDOM slope between data sets [51].

4. Results

The obtained results correspond to two topics: (i) thematic maps derived from images that represent an interesting approach to the near real-time monitoring of water quality, very valuable from the point of view of inland waters management, and (ii) field data that display the anomalies in the relationships between the [Cla] data and turbidity data, based on which a radiometric water quality field data campaign was planned and the existence of non-algal particulate matter (NAP) was identified.

4.1. Thematic Maps from Images

The first results were obtained from the atmospheric correction in which the reflectance values in the lagoon were low (visible bands from the OLI sensor). From these results, the algorithms were developed with the water dataset provided by the IMIDA team ([Cla] and turbidity) and visible spectral bands. The second step was the validation of these algorithms with other water datasets (Figure 2):

$$\text{Turbidity (NTU)} = 1.7746 \cdot \exp\{9.1066[(\text{Ref}_{\text{GREEN}} - \text{Ref}_{\text{RED}})/\text{Ref}_{\text{GREEN}} + \text{Ref}_{\text{RED}})]\} \qquad R^2 = 0.775$$

$$[\text{Cla}]\ (\text{mg/m}^3) = 0.6386 \cdot \exp\{4.7513[(\text{Ref}_{\text{GREEN}} - \text{Ref}_{\text{BLUE}})/\text{Ref}_{\text{GREEN}} + \text{Ref}_{\text{BLUE}})]\} \qquad R^2 = 0.8867$$

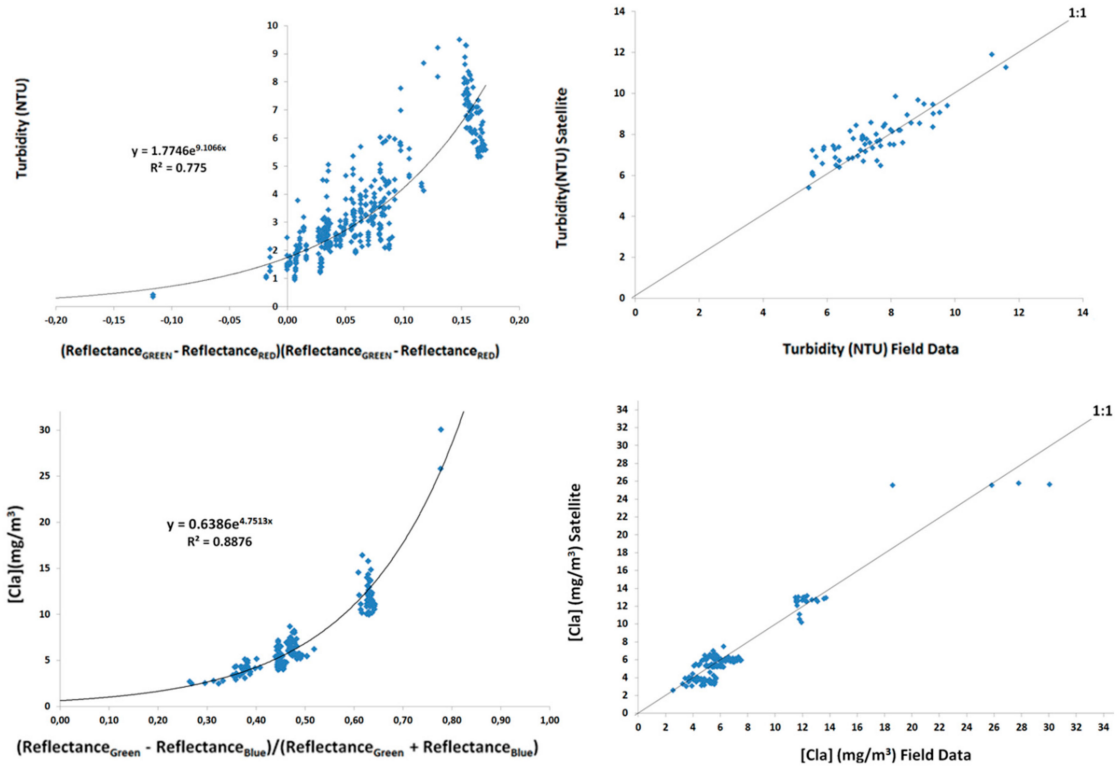

Figure 2. Relationships between water quality parameters and visible spectral bands, and their validation.

The second type of result is a set of atmospherically corrected OLI images from June 2015 to October 2017, and their corresponding turbidity and [Cla] thematic maps (Figures S1–S3 Supplementary Materials).

4.2. Field Data Results

This section includes the several types of results obtained in the field campaigns, while a discussion of the results is included in the following section:

- Turbidity and [Cla] time series from turbidimeter and fluorometer measurements in the first meter of depth are presented in Figure 3. Minimum values (around 2 mg m^{-3}) of chlorophyll-a were frequent during summer 2017, whereas maximum values (up to 37 mg m^{-3}) were recorded in January 2017, when storms resulted in the inflow of nutrients to the Mar Menor. Maximum values of turbidity were recorded in October 2016; minimum values also were recorded in summer 2017.
- Table 1 and Figures 4 and 5 summarize the ground data measurements from the field campaigns on 2 April 2017, the apparent optical properties, and the water absorption coefficient a (λ), as well as the analysis of the phytoplankton, mainly formed by an assemblage of some large diatoms and dinoflagellates (Figure S4).

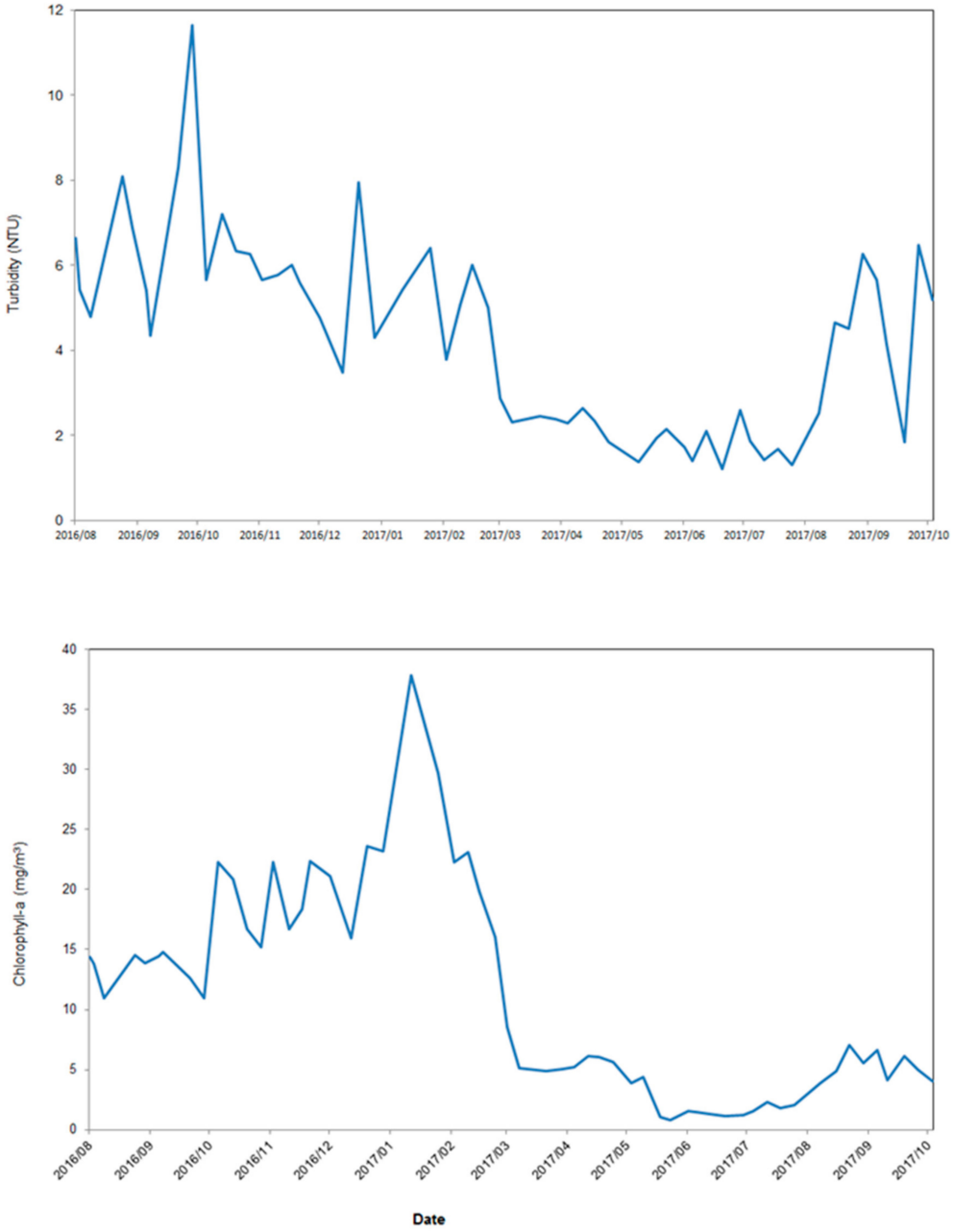

Figure 3. Turbidity in Nephelometric Turbidity Units (NTU) and chlorophyll-a concentration (mg/m^3) time series.

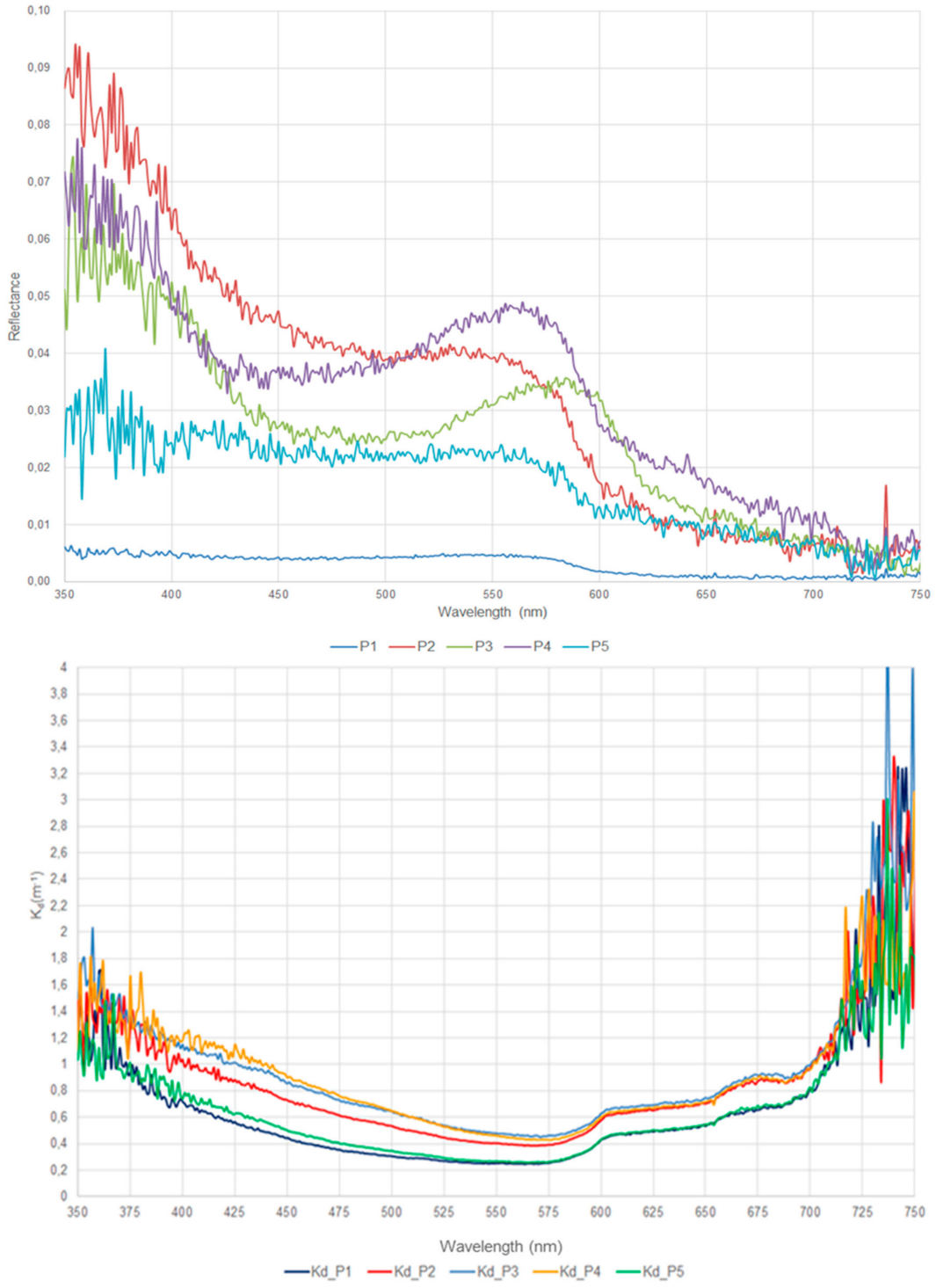

Figure 4. The water apparent optical properties recorded on 2 April 2017 in five point samplings, as in Table 1.

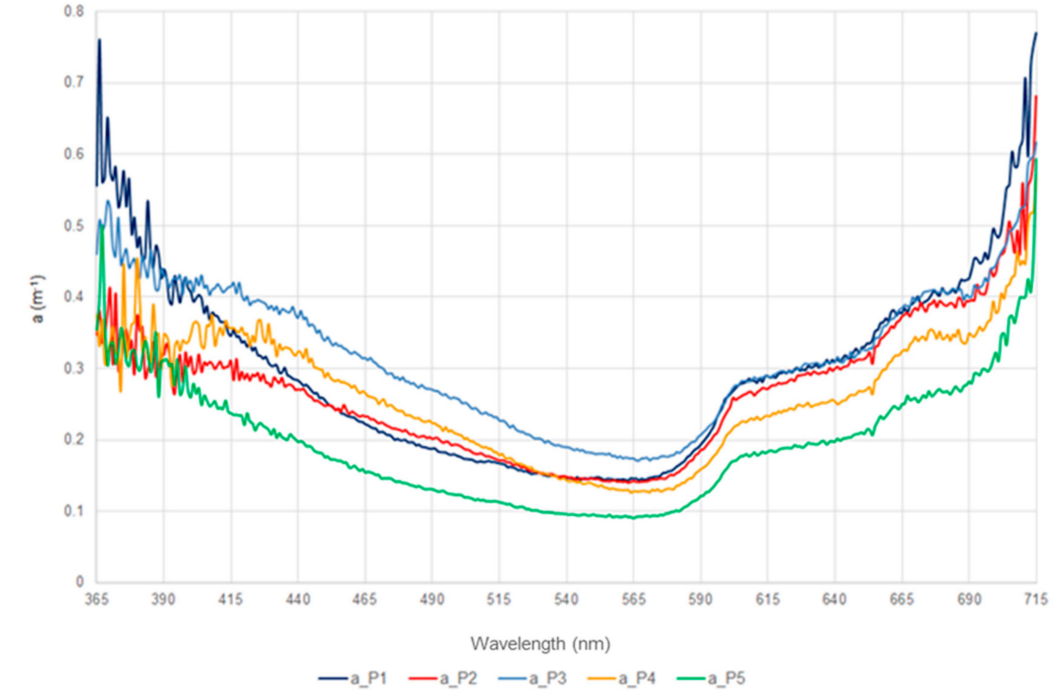

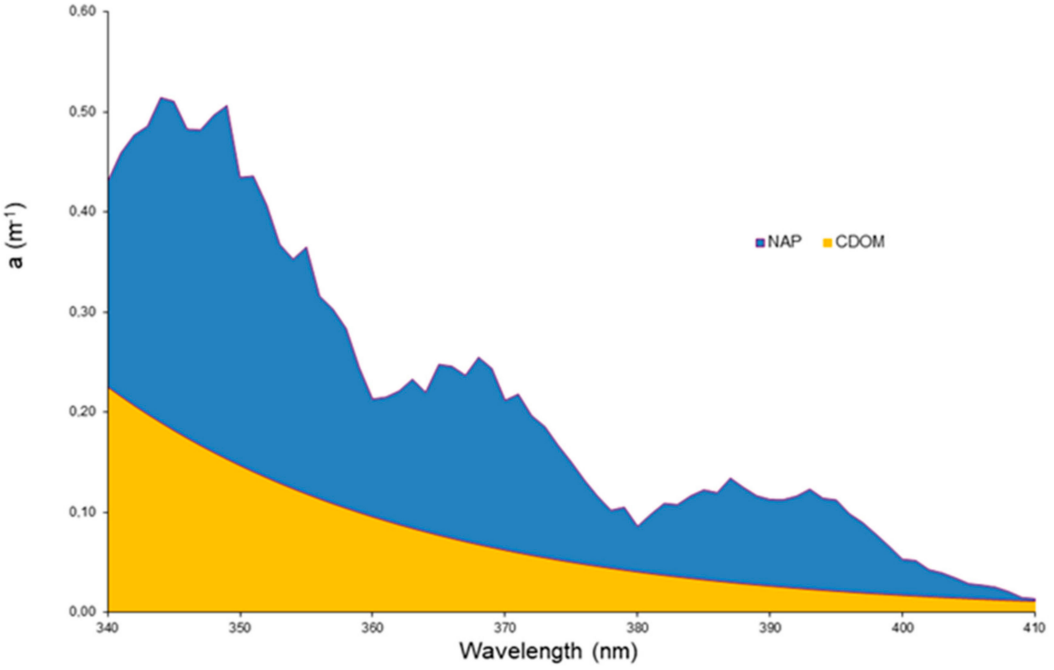

Figure 5. Water absorption coefficients, a (λ), estimated from apparent optical properties measured on 2 April 2017. The study of the water absorption coefficients allowed the determination of the colored dissolved organic matter (*CDOM*) absorption coefficient, acdom (λ), and the non-algal particles (NAP) absorption coefficient, anap(λ). The anap (λ) shows that there is other matter which interacts with the rest of the water components.

Table 1. Field data recorded on 2 April 2017 in five point samplings. Hours in Central European Time; coordinates in Universal Transverse Mercator system; depth of sampling point; SD, transparency measured as Secchi Disk depth vision.

Point	Date	Hour	X Coordinate	Y Coordinate	Depth (m)	SD (m)	Temperature (°C)	[Cla] (mg/m^3)	Turbidity (NTU)
1	2 April 2017	12:15	697406	4180918	5.8	5.4	24.7	0.2	0.37
2	2 April 2017	12:54	695285	4182202	6.3	2.9	26.2	1.2	0.64
3	2 April 2017	13:27	693926	4182881	3.5	1.9	24.2	4.8	1.25
4	2 April 2017	14:04	692664	4180696	5.6	1.4	23.5	2.1	2.55
5	2 April 2017	14:50	696646	4177782	6.8	2.9	22.4	0.1	0.21

5. Discussion

The analysis of the results has to be understood as part of the dynamic relationship between the water managers and remote sensing researchers. The social pressure due to the environmental degradation problems of the Mar Menor Lagoon caused the water managers to enquire about all the possible sources of information on the subject, so that they could understand the problem and find suitable solutions. The remote sensing techniques provide historical information that could be connected with the present datasets, thereby increasing our knowledge and supporting the decision-making process in order to solve the water pollution problem. The continuous and fast decline in the water quality of the lagoon caused planning decisions to be made close to real-time. Finally, the phases of the Mar Menor water quality monitoring project, using satellite images acquired during 2017, can be summarized as follows:

(1) Planning period (January–February). During this time, the economic feasibility of the project was analyzed, because, at this time, Spain was recovering from a huge economic crisis that imposed the need to act with caution regarding public investment and undertake only those projects that could be really useful. However, the tool to be used in this case (free satellite images, although without discounting the purchase of some images if there were no free ones available for a long period of time) to monitor the water quality in the lagoon enabled the managers to embark on the project with a minimum cost.

(2) Image processing period and methodology (March–May). The methodology applied to process the images was established in this period (Figure 2), during which some images obtained between 15 May 2015 and February 2017 were processed and the first thematic maps were generated (Figures S1–S3). These images were selected in order to have a general but appropriate view of the scope of the problem and the actual situation. The variables selected for the study were the [Cla], as a biomass parameter, and the turbidity, as a biochemical parameter. From the field campaign dataset and the multispectral images of the Landsat 8 satellite (corrected for reflectance), the algorithms were determined and the errors of the maps were identified, being considered suitable for remote sensing monitoring. The spectra of the images of this first phase indicated that the concentration of suspended solids was low and therefore the selected variables were suitable, since suspended solids were not an important factor in the study. In addition, the analysis of spatial changes indicated that there were the following types of water:

- Type 1: Low values of [Cla] and turbidity. This is considered to be the natural state of the water in the lagoon, and this situation corresponded to 15 May 2015.
- Type 2: High values of turbidity and low [Cla], as observed in the maps of 7 June 2015.
- Type 3: High values of [Cla] and turbidity, as seen in the image of 1 January 2016.

This visual analysis raised the need for a statistical study of the thematic cartography (Figure 6). The dates on which the values of turbidity and [Cla] were maximal coincide. However, the behavior of the minimum values was different, as can be observed in the period from 28 January 2017 to 9 April 2017. The behavior during this period of the maximum, minimum, and mean values differed between

turbidity and [Cla]. A clear absence of a relationship between these two parameters made it necessary to analyze the field data; this revealed two types of relationship between turbidity and [Cla] (Figure 7). Based on this result, an extra field data campaign was planned, with the aim of identifying the cause of this situation.

Figure 6. Time series of the maximum, minimum, and mean values of water parameters, estimated from satellite images.

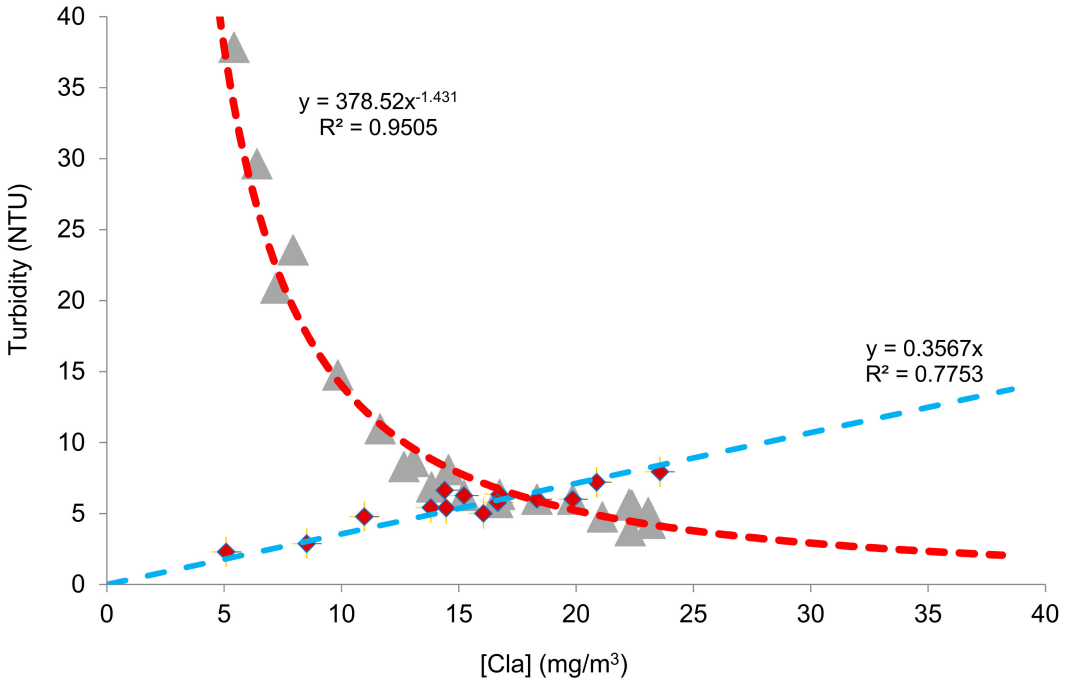

Figure 7. Different relationship between turbidity and [Cla]. Blue line, linear correlation between the variables; red line, inverse exponential relationship, where the turbidity is probably due to the presence of non-algal particles (NAP).

(3) Analysis period (March–June 2017). Monitoring by remote sensing was extended to all available images, since Landsat 8 passes through the study area every seven or nine days. We present the composition of the thematic maps in the Supplementary Materials Figures S1–S3. From this spatial information, an evolution that confirmed the results of the development phase was observed in the month of March of 2017: after the bloom in mid-January 2017, [Cla] decreased, but the turbidity was high by the end of January. There were no Landsat 8 images without clouds in February; therefore, no information on the lagoon was available. However, the atmospheric conditions were very dynamic, which promoted vertical movement in the water column and kept values of turbidity and [Cla] low at the beginning of March 2017. The image of 8 March 2017 shows that the values of [Cla] and turbidity were low, which indicates that the substance that had produced the high turbidity at the beginning of March had disappeared or was deposited on the bottom. In mid-March, some atmospheric dynamics were observed in the images because of the clouds that appeared over the lagoon. The image of 17 March 2017 shows an increase in the turbidity in the southern area of the lagoon, which was not caused by biomass. The images indicate that, in addition to phytoplankton, there was something on the bottom of the lagoon that dissolved in the water and underwent vertical movement with upward and downward dynamics in the water column, since the satellite observed the first optical thickness that, in the case of the Mar Menor, coincides with the first meter of the water column. The existence of more phytoplankton in the first meter of the water column is clearly shown in the images of 1 April 2017, when the value of the turbidity was much higher than that of [Cla]. In mid-April, the situation was reversed, and the turbidity was mainly due to the [Cla]. During the remainder of the month of April this situation prevailed, and large phytoplankton species—mainly dinoflagellates—predominated in the water (see Supplementary Materials Figure S4).

From the measurements of 2 April, and considering the location of the sampling points defined from the analysis of the images, the following conclusions are obtained (Table 1, Figures 4 and 5):

- There is no influence from the bottom, as was observed in the previous field campaigns of the IMIDA team.
- The reflectance values correspond to the visible range; thus, the algorithms of water parameters have to be defined in the spectral range (Figure 4), as they were developed in the second step (Figure 2).
- There are several areas in which natural marine water may be considered (point P1), where the reflectance and diffuse attenuation coefficient values are lowest, and the SD values are highest.
- The point P3 corresponds to zones where the principal component is the phytoplankton; it is defined by [Cla].
- There are several zones, where the principal components are the CDOM and NAP, in which the [Cla] is low and *SD* has a moderate value (point P5).
- The point P4 corresponds to areas where the phytoplankton value is higher than those of CDOM and NAP. The point P2 corresponds to areas where the CDOM and NAP values are higher than that of phytoplankton.
- The previous conclusions allow determination of the absorption coefficients of all the points and the estimation of the CDOM and NAP absorption coefficients.

During May 2017, the values of both recorded parameters were low again, which caused an increase in turbidity at the beginning of that month. The idea of the deposit on the bottom and its vertical movement was consolidated, based on an analysis of the maps of 5 June and 13 September. It was observed that these maps corresponded to cloudy days, when the atmospheric weather connects with water and moves it with more power in three-dimensional (3D) directions.

The relationship between turbidity and [Cla] was analyzed using the data obtained in the various campaigns and maps, and we concluded that there are two behaviors: one that evidences a clear relationship between turbidity and [Cla] (when [Cla] increases, so does turbidity) and another in which an increase in turbidity produces a decrease in [Cla] (Figure 7) through extinction of light and low photosynthesis. These behaviors suggest, as a hypothesis, the existence of a toxic compound in the water and the relevant tests were carried out, but the results for toxic substances were negative. Once this most dangerous possibility had been discounted, the existence of cyanobacteria was considered, and so a phytoplankton study was carried out; this algal group was found only in the southern part of the Mar Menor as small cells of *Synechococcus* sp.

Based on the reflectance spectra and the diffuse attenuation coefficient, the Mar Menor water was classified into four types: pure water from the lagoon; water in which phytoplankton predominates; water with a predominance of yellow organic matter; and water in which another type of matter predominates. From the spectral analysis, the absorption spectrum of the yellow matter dissolved in the Mar Menor water was obtained, as well as that of NAP. Determination of the elements that form NAP is a difficult task, due to the interaction between the multiple elements present in the water column and the bottom of the lagoon.

(4) Technical conclusions period (July–September). During the months of July and August 2017 the observed values of turbidity and [Cla] were low, increasing in September due to the predominance of phytoplankton being replaced by that of CDOM and NAP. In these months, there was evidence in the water quality of the behavior of a continental coastal water body, the values of [Cla] being much higher than those in marine waters. The name of the lagoon (Mar Menor, "Small Sea") reminds us that it is a coastal lagoon with values corresponding to the behavior of this type of water mass, which is different from the behavior of the water of the Mediterranean Sea. During this period, the phytoplankton composition changed from hundreds of individuals of large species to nanoplankton present in thousands per milliliter.

(5) Evaluation period (October–December). The project was analyzed by the managers, who evaluated the results obtained, the delivery of the results in the planned term, the effectiveness of the tool, and the economic cost. The evaluation was positive, which is why it is considered necessary

to continue with the elaboration of the thematic cartography and to carry out new planning in further years, to develop the monitoring by means of satellite images and to incorporate new techniques, platforms, and sensors.

The water managers involved in this study asked about the NAP composition and its provenance; however, none of these questions could be answered conclusively. NAP includes heterotrophic organisms, such as bacteria, micrograzers, and viruses [52], detrital organic particles, such as fecal pellets and cell debris, and mineral particles of both biogenic (e.g., calcite liths and shells) and terrestrial origin. It should be remembered that the total *NAP* absorption spectrum tends to increase monotonically as the wavelength decreases, in a way similar to that observed for CDOM [52]. The NAP in the Mar Menor has two possible origins: the effects of Saharan dust and the entry of suspended material (from runoff) during flash floods.

Despite Spanish meteorological agency reports about the effects of Saharan dust in Spain [53], the present study demonstrates that the effects of this dust were not coincident with the turbidity anomalies. However, flash floods around the Mar Menor [54] are considered the more probable cause because the level of the water exceeded 100 mm in 24 h several times, causing serious damage to infrastructures and buildings in lands close to the Mar Menor. New field data campaigns involving the collection of sediment samples have been planned, to shed light on the NAP composition

6. Conclusions

Social pressure forced the managers to evaluate different techniques that could reveal the causes of the water color change of the Mar Menor coastal lagoon and, consequently, the trophic state, as well as their evolution over time.

The analysis of multispectral images allows the temporal monitoring of a water body, as happened in Mar Menor. The methodology developed allows us to use images from the Landsat series, so the study could be extended to the past by using the first images of the area captured by this series of Earth observation satellites in the 1970s, with a periodicity between seven and nine days in this area. Simultaneously, a quasi-real-time monitoring system has been created, through which the processing time has been optimized to less than an hour, depending on the cloud cover. That is, once the satellite image is available, and until maps of water quality variables are obtained, less than 1 h elapses during the processing of the image and its incorporation into the water quality monitoring system of the Mar Menor, to which the managers have technical access. However, the time between the moment when the sensor acquires the image and the moment when it is uploaded onto the website is variable, between eight and 48 h. Depending on this, the maps will be ready, in the best of cases, on the night following the day of acquisition of the image. These problems will be solved by incorporating into the management system the images of the new sensors of the ESA Sentinel satellites and their distribution through the Copernicus program.

Spatial remote sensing has detected that turbidity in the Mar Menor is not caused only by phytoplankton; there are also chemical compounds involved, which have not been identified (CDOM and NAP), although in this work we have obtained their spectral absorption signatures. We do not know their origin, although—dissolved in the water—they have reached the bottom in such amounts that the internal currents cause a vertical displacement in the water column that started to be detected in June 2015. These substances interact with phytoplankton, causing an excessive increase in [Cla], which was observed for the first time in the image of 1 January 2016. We must not forget that on dates before June 2015, the values of [Cla] were similar to those in the Mediterranean Sea, but in June 2015 the change in apparent color from blue to green began, being so obvious by the end of 2015 and early 2016 that it caused social alarm, although on several occasions the green color has changed to blue (on those dates when the maximum values of [Cla] and turbidity were very low). These color changes are produced because of the movement of phytoplankton, CDOM, and NAP in the water column. However, the social alarm, the factor that made the managers take the decision to initiate various actions in this ecosystem for its conservation and improvement, has not stopped at any time.

The objective of this work has been fulfilled by providing answers to the questions of the managers and generating a methodology to determine the water quality in the Mar Menor that has been incorporated into an operational monitoring system that functions in real-time and is spatially distributed. The tracking system using satellite images is open to the incorporation of images from new multispectral sensors.

Within the IDEARM project (Design and implementation of spatial data infrastructure (SDI) on agriculture and water in the Region of Murcia), a thematic geoportal is being developed that includes remote sensing data from Campo de Cartagena and the Mar Menor. The geoportal is intended to integrate the altimetry and bathymetric information available from the different producer organizations, the objectives being the compilation of the historical series of altimetry available for the study area and the development of a platform that allows the spatial and temporal monitoring of the Mar Menor. The viewer of the project that is being developed will be able to integrate information from satellite images (Landsat 8, Sentinel II, Spot 7, Pleiades, and Deimos), aerial photographs from different civil and military flights, and photogrammetry and bathymetric data obtained by different national and regional agencies. The geoportal developed within the project IDEARM integrates datasets from various government bodies which have in common a spatial component that allows their localization in the territory. In this sense, the Infrastructure for Spatial Information in the European Community (INSPIRE) directive has been applied as a framework. Furthermore, a spatial data infrastructure based on Open Geospatial Consortium (OGC) services has been built to query and manage useful information, especially for the Mar Menor communities, becoming a support tool in decision-making for environmental monitoring.

The viewer uses the application programming interface (API) of ArcGIS for Adobe Flex, which provides the basis of a web application that includes the following services: map viewer, geocoding, metadata access, and geoprocessing based on the ESRI ArcGIS Server. The abovementioned ArcGIS API for Adobe Flex allows us to develop high-performance applications that deliver GIS content and functionality for geo-portal users (https://geoportal.imida.es/agua/), as presented in Figure 8.

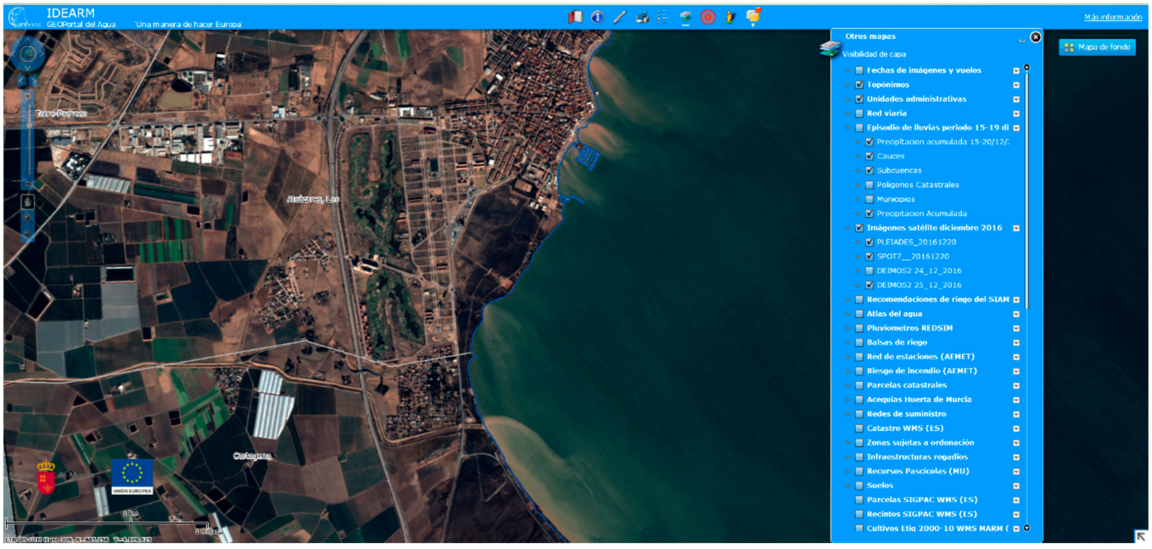

Figure 8. Initial screen (in Spanish) of the IMIDA geoportal.

Supplementary Materials: The Supplementary Materials are available online at http://www.mdpi.com/2073-4441/11/7/1468/s1.

Author Contributions: The co-authors contributed in similar proportions to the work. The main author (M.E.) developed the conceptualization and methodology, and contributed to all sections of the work. J.A.D. and S.G.-G. contributed to the writing, review, and editing. F.A. and J.S. contributed to the design of the experiments.

Funding: This research was co-funded (80%) by the European Regional Development Fund (ERDF), through grant number FEDER 14-20-15.

Conflicts of Interest: The authors declare no conflict of interest.

References

1. Northrop, A. *IDEAS—LANDSAT Products Description Document*; IDEAS-VEG-SRV-REP-1320; IDEAS; Telespazio VEGA UK Ltd.: Luton, UK, 2015.
2. López, M.J.; Caselles, V. A multitemporal study of chlorophyll-a concentration in the Albufera lagoon of Valencia, using Thematic Mapper data. *Int. J. Remote Sens.* **1990**, *11*, 301–311. [CrossRef]
3. Domínguez, J.A.; Chuvieco, E.; Sastre, A. Monitoring transparency in inland water bodies using multispectral images. *Int. J. Remote Sens.* **2009**, *30*, 1567–1586. [CrossRef]
4. Evenson, E.J.; Orndorff, R.C.; Blome, C.D.; Böhlke, J.K.; Hershberger, P.K.; Langenheim, V.E.; McCabe, G.J.; Morlock, S.E.; Reeves, H.W.; Verdin, J.P.; et al. *Strategic Directions for U.S. Geological Survey Water Science, 2012–2022—Observing, Understanding, Predicting, and Delivering Water Science to the Nation—Public Review Release*; USGS Open-File Report; US Geological Survey: Reston, VA, USA, 2012; No. 2012–1066.
5. Erena, M.; Atenza, J.F.; García-Galiano, S.; Domínguez, J.A.; Bernabé, J.M. Use of Drones for the Topo-Bathymetric Monitoring of the Reservoirs of the Segura River Basin. *Water* **2019**, *11*, 445. [CrossRef]
6. Gilabert, M.A.; Conese, C.; Maselli, F. An atmospheric correction method for the automatic retrieval of surface reflectances from TM images. *Int. J. Remote Sens.* **1994**, *15*, 2065–2086. [CrossRef]
7. Ruiz, L.J.; Estornell, J.; Erena, M. Monitoring of the Water Quality of the Picadas Reservoir Using Landsat 8 Images (September 2015–December 2016). Remote Sensing: New platforms and sensors applied to the management of water, agriculture and the environment. 2017. In Proceedings of the XVII Congreso de la Asociación Española de Teledetección 2017, Murcia, Spain, 3–7 October 2017.
8. Domínguez, J.A.; Vargas, J.; Alonso, A. Remote sensing as a tool for monitoring water quality parameters for Mediterranean Lakes of European Union water framework directive (WFD) and as a system of surveillance of cyanobacterial harmful algae blooms (SCyanoHABs). *Environ. Monit. Assess.* **2011**, *181*, 317–334.
9. Flener, C.; Vaaja, M.; Jaakkola, A.; Krooks, A.; Kaartinen, H.; Kukko, A.; Kasvi, A.; Hyyppä, H.; Hyyppä, H.; Alho, P. Seamless Mapping of River Channels at High Resolution Using Mobile LiDAR and UAV-Photography. *Remote Sens.* **2013**, *5*, 6382–6407. [CrossRef]
10. Castillo-López, E.; Dominguez, J.A.; Pereda, R.; de Luis, J.M.; Pérez, R.; Piña, F. The importance of atmospheric correction for airborne hyperspectral remote sensing of shallow waters: Application to depth estimation. *Atmos. Meas. Tech.* **2017**, *10*, 3919–3929. [CrossRef]
11. Blondeau-Patissier, D.; Gower, J.; Dekker, A.; Phinn, S.; Brando, V. A review of ocean color remote sensing methods and statistical techniques for the detection, mapping and analysis of phytoplankton blooms in coastal and open oceans. *Prog. Oceanogr.* **2014**, *123*, 123–144. [CrossRef]
12. Mushtaq, F.; Lala, M. Remote estimation of water quality parameters of Himalayan lake (Kashmir) using Landsat 8 OLI imagery. *Geocarto Int.* **2016**, *32*, 274–285. [CrossRef]
13. Xiong, J.; Thenkabail, P.S.; Tilton, J.C.; Gumma, M.K.; Teluguntla, P.; Oliphant, A.; Congalton, R.G.; Yadav, K.; Gorelick, N. Nominal 30-m Cropland Extent Map of Continental Africa by Integrating Pixel-Based and Object-Based Algorithms Using Sentinel-2 and Landsat-8 Data on Google Earth Engine. *Remote Sens.* **2017**, *9*, 1065. [CrossRef]
14. Reillon, V. *Securing the Copernicus Programme Why EU Earth Observation Matters*; PE 599.407; European Parliamentary Research Service: Brussels, Belgium, 2017.
15. Matthews, M. A current review of empirical procedures of remote sensing in inland and near-coastal transitional waters. *Int. J. Remote Sens.* **2011**, *32*, 6855–6899. [CrossRef]
16. Pu, P.; Chen, L.; Hu, R. Evaluating recommender systems from the user's perspective: Survey of the state of the art. *User Model. User-Adap. Interact.* **2012**, *22*, 317. [CrossRef]
17. Concha, J.; Schott, J. Retrieval of colour producing agents in Case 2 waters using Landsat 8. *Remote Sens. Environ.* **2016**, *185*, 95–107. [CrossRef]
18. Chao, Y.; el Anjoumi, A.; Domínguez, J.A.; Rodríguez, D.; Rico, E. Using Landsat image time series to study a small water body in Northern Spain. *Environ. Monit. Assess.* **2014**, *186*, 3511–3522.

19. Eleveld, M.; Ruescas, A.; Hommersom, A.; Moore, T.; Peters, S.; Brockmann, C. An Optical Classification Tool for Global Lake Waters. *Remote Sens.* **2017**, *9*, 420. [CrossRef]
20. Spyrakos, E.; O'Donnell, R.; Hunter, P.D.; Miller, C.; Scott, M.; Simis, S.G.; Neil, C.; Barbosa, C.C.; Binding, C.E.; Bradt, S.; et al. Optical types of inland and coastal waters. *Limnol. Oceanogr.* **2018**, *63*, 846–870. [CrossRef]
21. Navarro, G.; Caballero, I.; Vazquez, A. Sentinel-2 Imagery for Tuna Fishing Management. *Sea Technol.* **2017**, *57*, 29–31.
22. Toming, K.; Kutser, T.; Uiboupin, R.; Arikas, A.; Vahter, K.; Paavel, B. Mapping Water Quality Parameters with Sentinel-3 Ocean and Land Colour Instrument Imagery in the Baltic Sea. *Remote Sens.* **2017**, *9*, 1070. [CrossRef]
23. Dörnhöfer, K.; Klinger, P.; Heegeb, T.; Oppelt, N. Multi-sensor satellite and In Situ monitoring of phytoplankton development in a eutrophic-mesotrophic lake. *Sci. Total Environ.* **2018**, *612*, 1200–1214. [CrossRef]
24. Marin, A.; Lloret, J.; Velasco, J.; Bello, C. The physio-geographical background and ecology of Mar Menor. In *Coastal Lagoons in Europe: Integrated Water Resource Strategies*; Lillebo, A.I., Stalnacke, P., Gooch, G.D., Eds.; IWA Publishing: London, UK, 2015; pp. 39–46.
25. Pérez-Ruzafa, A.; Marcos, C.; Gilabert, J. The ecology of the Mar Menor coastal lagoon: A fast changing ecosystem under human pressure. In *Coastal Lagoons. Ecosystem Processes and Modeling for Sustainable Use and Development*; Gönenc, I.E., Wolflin, J.P., Eds.; CRC Press: Boca Raton, FL, USA, 2005.
26. Robledano, F.; Esteve, M.A.; Calvo, J.F.; Martínez-Paz, J.M.; Farinós, P.; Carreño, M.F.; Soto, I.; Avilés, M.; Ballesteros, G.A.; Martínez-Baños, P.; et al. Multi-criteria assessment of a proposed ecotourism, environmental education and research infrastructure in a unique lagoon ecosystem: The Encañizadas del Mar Menor (Murcia, SE Spain). *J. Nat. Conserv.* **2018**, *43*, 201–210. [CrossRef]
27. Díaz, A.R.; Pedraza, A.C.; Morales, A.P. Expansión urbana y turismo en la Comarca del Campo de Cartagena-Mar Menor (Murcia). Impacto en el sellado del suelo. *Cuad. Tur.* **2017**, *39*, 521–546. [CrossRef]
28. Castejón-Porcel, G.; Espín-Sánchez, D.; Ruiz-Álvarez, V.; García-Marín, R.; Moreno-Muñoz, D. Runoff Water as A Resource in the Campo de Cartagena (Region of Murcia): Current Possibilities for Use and Benefits. *Water* **2018**, *10*, 456. [CrossRef]
29. García-Ayllón, S. Diagnosis of complex coastal ecological systems: Environmental GIS analysis of a highly stressed Mediterranean lagoon through spatiotemporal indicators. *Ecol. Indic.* **2017**, *83*, 451–462. [CrossRef]
30. Leon, V.M.; Bellido-Millán, J.M. (Eds.) *Mar Menor: Una Laguna Singular y Sensible. Evaluación Científica de su Estado*; Instituto Español de Oceanografía: Madrid, Spain, 2016; 343p.
31. La Verdad de Murcia. Denuncian el Color Verde del Mar Menor. 2018. Available online: https://www.laverdad.es/murcia/denuncian-color-verde-20170810004013-ntvo.html (accessed on 28 May 2018).
32. Morel, A.; Gentili, B. Diffuse reflectance of oceanic waters. II. Bidirectional aspects. *Appl. Opt.* **1993**, *32*, 6864–6879. [CrossRef] [PubMed]
33. Tyler, J. Radiance distribution as a function of depth in an underwater environment. *Bull. Scripps Ins. Oceanogr.* **1960**, *7*, 363–412.
34. Mobley, C.D. Estimation of the remote-sensing reflectance from above-surface measurements. *Appl. Opt.* **1999**, *38*, 7442–7455. [CrossRef] [PubMed]
35. Huang, C.; Yao, L. Semi-Analytical Retrieval of the Diffuse Attenuation Coefficient in Large and Shallow Lakes from GOCI, a High Temporal-Resolution Satellite. *Remote Sens.* **2017**, *9*, 825–838. [CrossRef]
36. Picazo, A.; Rochera, C.; Vicente, E.; Miracle, M.R.; Camacho, A. Spectrophotometric methods for the determination of photosynthetic pigments in stratified lakes: A critical analysis based on comparisons with HPLC determinations in a model lake. *Limnetica* **2013**, *32*, 139–158.
37. Fargion, G.S.; Mueller, J.L. *Ocean Optics Protocols For Satellite Ocean Color Sensor Validation, Revision 2*; NASA Goddard Space Flight Center Greenbelt: Greenbelt, MA, USA, 2000.
38. Shi, L.; Mao, Z.; Wu, J.; Liu, M.; Zhang, Y.; Wang, Z. Variations in Spectral Absorption Properties of Phytoplankton, Non-Algal Particles and Chromophoric Dissolved Organic Matter in Lake Qiandaohu. *Water* **2017**, *9*, 352. [CrossRef]
39. Doña, C.; Sánchez, J.M.; Caselles, V.; Domínguez, J.A.; Camacho, A. Empirical Relationships for Monitoring Water Quality of Lakes and Reservoirs through Multispectral Images. *IEEE J. Sel. Top. Appl. Earth Obs. Remote Sens.* **2014**, *7*, 1632–1641. [CrossRef]

40. Jaelani, L.; Limehuwey, R.; Kurniadin, N.; Pamungkas, A.; Koenhardono, E.; Sulisetyono, E. Estimation of TSS and Chl-a Concentration from Landsat 8-OLI: The Effect of Atmosphere and Retrieval Algorithm. *IPTEK J. Technol. Sci.* **2016**, *27*, 16–23. [CrossRef]
41. Quang, N.; Sasaki, J.; Higa, H.; Huan, N. Spatiotemporal Variation of Turbidity Based on Landsat 8 OLI in Cam Ranh Bay and Thuy Trieu Lagoon, Vietnam. *Water* **2017**, *9*, 570. [CrossRef]
42. Lymburner, L.; Botha, E.; Hestir, E.; Anstee, J.; Sagar, S.; Dekker, A.; Malthus, T. Landsat 8: Providing continuity and increased precision for measuring multi-decadal time series of total suspended matter. *Remote Sens. Environ.* **2016**, *185*, 108–118. [CrossRef]
43. Zlinszky, A.; Supan, P.; Koma, Z. Near real-time qualitative monitoring of lake water chlorophyll globally using GoogleEarth Engine. In Proceedings of the 19th EGU General Assembly, Vienna, Austria, 23–28 April 2017; Volume 19, p. 18950.
44. Simis, S.; Ruiz-Verdú, A.; Domínguez-Gómez, J.A.; Peña-Martinez, R.; Peters, S.; Gons, H. Influence of phytoplankton pigment composition on remote sensing of cyanobacterial biomass. *Remote Sens. Environ.* **2007**, *106*, 414–427. [CrossRef]
45. Singh, R.; Shanmugam, P. A Multidisciplinary Remote Sensing Ocean Color Sensor: Analysis of User Needs and Recommendations for Future Developments. *IEEE J. Sel. Top. Appl. Earth Obs. Remote Sens.* **2016**, *9*, 5223–5238. [CrossRef]
46. Groetsch, P.; Gege, P.; Simis, S.; Eleveld, M.; Peters, S. Validation of a spectral correction procedure for sun and sky reflections in above-water reflectance measurements. *Opt. Express* **2017**, *25*, 286475–286495. [CrossRef]
47. Kirk, J.T.O. *Light and Photosynthesis in Aquatic Ecosystem*, 1st ed.; Cambridge University Press: New York, NY, USA, 1994.
48. Roesler, C.S.; Perry, M.J. In Situ phytoplankton absorption, fluorescence emission, and particulate backscattering spectra determined from reflectance. *J. Geophys. Res.* **1995**, *100*, 13279–13294. [CrossRef]
49. Garver, A.H.; Siegel, D.A. Inherent optical property inversion of ocean color spectra and its biogeochemical interpretation: 1. Time series from the Sargasso Sea. *J. Geophys. Res.* **1997**, *102*, 18607–18625. [CrossRef]
50. Wang, P.; Boss, E.; Roesler, C. Uncertainties of inherent optical properties obtained from semianalytical inversions of ocean color. *Appl. Opt.* **2002**, *44*, 4074–4085. [CrossRef]
51. Kratzer, S.; Moore, G. Inherent Optical Properties of the Baltic Sea in Comparison to Other Seas and Oceans. *Remote Sens.* **2018**, *10*, 418. [CrossRef]
52. Bellacicco, M.; Volpe, G.; Briggs, N.; Brando, V.; Pitarch, J.; Landolfi, A.; Colella, S.; Marullo, S.; Santoleri, R. Global distribution of non-algal particles from ocean color data and implications for phytoplankton biomass detection. *Geophys. Res. Lett.* **2018**, *45*, 7672–7682. [CrossRef]
53. Pérez, N.; Querol, X.; Olivares, I.; Alastuey, A.; Hervás, M.; Cornide, M.J.; Javato, R.; Salvador, P.; Artíñano, B.; de la Rosa, J. *Natural Particle Episodes 2017*; The Spain Ministry of Agriculture and Fisheries: Madrid, Spain, 2018.
54. Espín Sánchez, D.; García Lorenzo, R.; Ruiz Álvarez, V.; Conesa García, C. The heavy rains and floods on 17 and 18 December 2016 in the Region of Murcia, with particular focus on the Mar Menor Watershed. *Ing. Agua* **2017**, *21*, 213–229. [CrossRef]